Considerations on the design of sectored receivers for wireless optical channels using a Monte-Carlo-based ray-tracing algorithm

Article *in* IET Optoelectronics · November 2007

DOI: 10.1049/iet-opt:20060062 · Source: IEEE Xplore

5 authors, including:

Beatriz Rodríguez Mendoza
Universidad de La Laguna

Sarahaime Rodriguez
Pontificia Universidad Católica Madre y Maestra

Rafael Pérez-JImenez
Universidad de Las Palmas de Gran Canaria

Enrique Poves
University of Strathclyde

Considerations on the design of conventional receivers for wireless optical channels using a Monte Carlo based ray-tracing algorithm

S. Rodríguez*[a], B.R. Mendoza [a], O. González [a], A. Ayala [a], R. Pérez Jiménez [b]
[a] Laboratorio de Comunicaciones, Facultad de Física, Univ. de La Laguna, 38203, Tenerife, Spain
[b] Dept. de Señales y Comunicaciones, Univ. de Las Palmas de G.C., 35015, Gran Canaria, Spain

ABSTRACT

This paper presents a study of the design of a conventional receiver structure that offers improved performance with respect to the main IR channel parameters, such as path loss and *rms* delay spread. To this end, we use a recently proposed model for the effective signal-collection area of a conventional angle-diversity receiver that is nearer to real behaviour than the ideal model. The inclusion of this model in the Monte Carlo ray-tracing algorithm allows us to study those optical links that are characterized by the use of these receivers and investigate the structure of the conventional receiver that yields improve performance with respect to the IR channel parameters. Based on the obtained results, we propose the use of a conventional receiver composed of seven branches o photodiodes. One oriented towards the ceiling, and six looking at an elevation of 56º with a separation of 60º in azimuth. For each element, a CPC with a FOV=50º must be used. Furthermore, the proposed structure is evaluated in a representative link budget using L-PPM modulation schemes.

Keywords: Infrared channel, conventional receiver, angle-diversity, ray-tracing.

1. INTRODUCTION

Non-directed infrared (IR) radiation has been considered as a very attractive alternative to radio frequency (RF) waves for indoor wireless local area networks. However, there are two major limitations for establishing a wideband infrared communications link: the power requirements and the intersymbol interference caused by multipath dispersion. In general, the use of multibeam transmitter in conjunction with angle-diversity receivers makes it possible to reduce the impact of ambient light noise, path loss and multipath distortion, in part by exploiting the fact that they are often received from different directions than the desired signal. Basically, there are three ways to get angle-diversity detection[1]: using conventional, imaging or sectored receivers. A conventional receiver uses multiple photodiodes that are oriented in various directions[2,3], an imaging diversity receiver is composed of an optical concentrator that focuses on a segmented photodetector array[4,5], and finally, a sectored receiver is a hemisphere where a set of parallels and meridians defines the photodetector boundaries[6].

The propagational characteristics of the indoor infrared channel are fully described by the channel impulse response, which depends on multiple factors such as the room geometry, the reflection pattern from the various surfaces, the emitter and receiver characteristics and their relative locations. In order to estimate the impulse response on IR wireless indoor channels, several simulation methods have been put forth[7,8], but all of them share the same problem, namely, the intensive computational effort. However, a Monte Carlo ray-tracing algorithm was proposed, which presents a lower computational cost than previous methods[9,10]. Indoor optical channel simulation can significantly enhance the design of angle-diversity receivers, but requires models that correctly fit the receiver characteristics. To this end, we use a recently proposed model for the effective signal-collection area of a conventional angle-diversity receiver that is nearer to real behaviour than the ideal model. In this model, each receiving element utilizes its own nonimaging concentrator, such as a Compound Parabolic Concentrator (CPC). The inclusion of this model in the Monte Carlo ray-tracing algorithm allows us to study those optical links that are characterized by the use of these receivers.

*srdguezp@ull.es; phone 34 922 845042.

VLSI Circuits and Systems IV, edited by Teresa Riesgo, Eduardo de la Torre, Leandro Soares Indrusiak,
Proc. of SPIE Vol. 7363, 736316 · © 2009 SPIE · CCC code: 0277-786X/09/$18 · doi: 10.1117/12.821733

This paper investigates the structure of the conventional receiver that yields improve performance with respect to the indoor IR channel characteristics. In Section 2, we describe the Monte Carlo ray-tracing algorithm used to evaluate the impulse response of the indoor IR channel. Section 3 describes the model used for the effective signal-collection area of a conventional receiver. In Section 4, the influence of receiver parameters on the channel characteristics are studied and the conventional receiver structure that offers the best performance with respect to the IR channel parameters is proposed. Finally, Section 5 outlines the conclusions of this work.

2. CHANNEL IMPULSE RESPONSE

In order to evaluate the impulse response of the indoor IR channel, a Monte Carlo ray-tracing algorithm was implemented. In general, the impulse response of the IR indoor channel for arbitrary emitter E and receiver R positions can be expressed as an infinite sum of the form:

$$h(t;E,R) = h^{(0)}(t;E,R) + \sum_{k=1}^{\infty} h^{(k)}(t;E,R) \tag{1}$$

where $h^{(k)}(t)$ is the impulse response of the light undergoing k reflections. The first term represents the line-of-sight (LOS) response, and the second one, the multiple-bounce impulse responses.

Given an emitter and receiver in an environment free of reflectors, with a large distance d between both, the LOS impulse response is approximately

$$h^{(0)}(t;E,R) = \frac{1}{d^2} R_E(\varphi,n)\, A_{eff}(\psi)\, \delta\left(t - \frac{d}{c}\right) \tag{2}$$

where $R_E(\varphi, n)$ represents the generalized Lambertian model used to approximate the radiation pattern of the emitter, c the speed of light and $A_{eff}(\psi)$ the effective signal-collection area of the receiver[7]. In an environment with reflectors, however, the radiation from the emitter can reach the receiver after any number of reflections (see Fig. 1). In the algorithm, to calculate the impulse response due to multiple reflections, many rays are generated at the emitter position with a probability distribution equal to its radiation pattern. The power of each generated ray is initially P_E/N, where N is the number of rays used to discretize the source. When a ray impinges on a surface, the reflection point becomes a new optical source, thus a new ray is generated with a probability distribution provided by the reflection pattern of that surface. The process continues throughout the maximum simulation time, t_{max}. After each reflection, the power of the ray is reduced by the reflection coefficient of the surface and the reflected power reaching the receiver ($p_{i,k,}$ ith ray, kth time interval) is computed by

$$p_{i,k} = \frac{1}{d^2} R_S(\phi,\phi')\, A_{eff}(\psi) \tag{3}$$

where $R_S(\phi,\phi')$ is the model used to describe the reflection pattern. In this work, Phong's model has been used[10]. This model is able to approximate the behaviour of those surfaces that present a specular component. Consequently, surface characteristics are defined by three parameters: the reflection coefficient ρ, the percentage of incident signal that is reflected diffusely r_d and the directivity of the specular component of the reflection m.

Therefore, the total received power in the kth time interval (width Δt) is calculated as the sum of the power of the N_k rays that contribute in that interval.

$$p_k = \sum_{i=1}^{N_k} p_{i,k} = \sum_{i=1}^{N_k} \frac{1}{d^2} R_S(\phi,\phi')\, A_{eff}(\psi) \tag{4}$$

Defining $M = t_{max}/\Delta t$, and assuming as the time origin the arrival of the LOS component, the impulse response after multiple reflections is given by

$$\sum_{k=1}^{\infty} h^{(k)}(t;E,R) = \sum_{j=0}^{M-1} p_k\, \delta(t - j\Delta t) \tag{5}$$

Replacing (2) and (5) in (1), the channel impulse response can be expressed as

$$h(t;E,R) = \frac{1}{d^2} R_E(\varphi,n) A_{eff}(\psi)\delta(t) + \sum_{j=1}^{M-1} p_k \delta(t - j\Delta t) \tag{6}$$

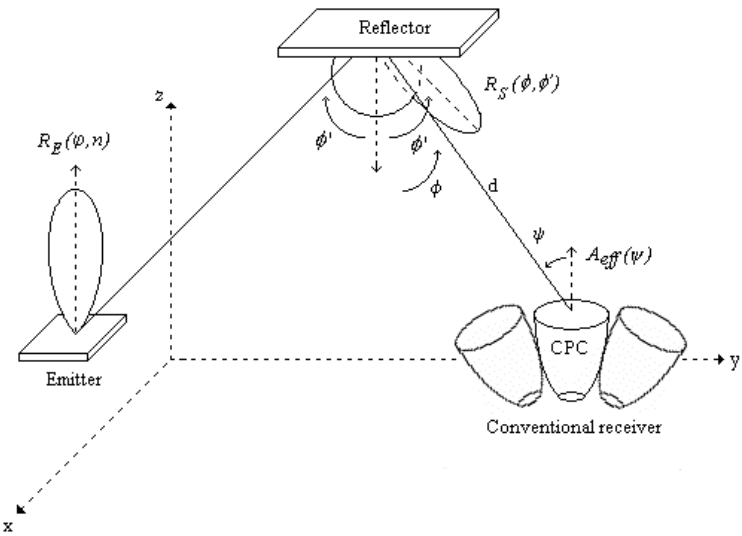

Fig. 1. Emitter and receiver geometry with reflectors. The surface reflection pattern is described by Phong's model.

3. EFFECTIVE SIGNAL-COLLECTION AREA MODEL

Achieving a high signal to noise ratio (SNR) is the goal for most infrared link applications. Noise from ambient infrared can be minimized by using optical filtering. Optical concentrators are used to increase the effective collection area of infrared receivers without requiring large-area detectors. For links that make use of a wide FOV (Field Of View), hemispherical lenses are recommended, while compound parabolic concentrators (CPC) are used for more direct links.

In general, a bare detector achieves an effective signal-collection area of

$$A_{eff}^{bare}(\psi) = A_R \cos(\psi) rect\left(\frac{\psi}{\pi/2}\right) \tag{7}$$

Adding a filter and concentrator, the effective signal–collection area of the receiver becomes

$$A_{eff}^{c,f}(\psi) = A_R T_S(\psi) g(\psi) \cos(\psi) rect\left(\frac{\psi}{\pi/2}\right) \tag{8}$$

where $T_S(\psi)$ is the filter transmission and $g(\psi)$ the concentrator gain. Nonimaging concentrators exhibit a trade-off between gain and FOV. An idealized nonimaging concentrator having an internal refractive index n achieves a constant gain expressed as

$$g(\psi) = \frac{n^2}{\sin^2 \psi_c} rect\left(\frac{\psi}{\psi_c}\right) \tag{9}$$

where ψ_c is the concentrator FOV (semi-angle). Usually, $\psi_c \leq \pi/2$. In our model, the concentrator gain is affected by the optical efficiency $\eta(\psi)$, which represents the reflection losses of the concentrator. Furthermore, the propagation delay introduced by the concentrator is considered[11].

$$g(\psi) = \frac{n^2}{sin^2\,\psi_c}\eta(\psi)\,rect\left(\frac{\psi}{\pi/2}\right) \tag{10}$$
$$t(\psi) \neq 0$$

Replacing $g(\psi)$ in the expression that defines the effective signal–collection area of the receiver, it can be expressed as

$$A_{eff}^{c,f}(\psi) = \frac{n^2 A_R\, T_S(\psi)\,cos(\psi)}{sin^2\,\psi_c}\eta(\psi)\;rect\left(\frac{\psi}{\pi/2}\right) \tag{11}$$

In a wireless infrared communications system, an optical bandpass filter can be used to limit the ambient radiation reaching the detector. A common form of band pass filter consists of a stack of dielectric thin-film layers. By properly choosing the number of layers, their thicknesses, and their refractive indexes, it is possible to control the surface reflectance and thus the filter transmittance. The filter transmission $T_S(\psi)$, can be described fairly accurately by a simple, five-parameter model[12]. In this model, for radiation of wavelength λ_o incident at angle ψ, the filter transmission is given by

$$T(\psi;\Delta\lambda,\psi') = \frac{T_0}{1+\left[\dfrac{\lambda_0-\lambda'(\psi;\psi')}{\Delta\lambda/2}\right]^{2m}} \tag{12}$$

where ψ' is the filter orientation, T_0 is the peak transmission at ψ', $\Delta\lambda$ is the spectral half-power bandwidth, m is the filter order and $\lambda'(\psi;\psi')$ represents the shifting to shorter wavelengths at nonnormal incidences, which is

$$\lambda'(\psi;\psi') = \lambda_0\left(\frac{n_s^2-n_1^2\,sen^2\psi}{n_s^2-n_1^2\,sen^2\psi'}\right)^{1/2} \tag{13}$$

where n_1 is the index of the input layer and n_s is an effective index for the spacer layer. The design of the optical filter thus boils down to specifying the two parameters $\Delta\lambda$ and ψ'. The remaining three parameters (n_s, m and T_0) are generally fixed by technology. Furthermore, to provide the best utilization of the CPC and filter, the angular bandwidth $\Delta\psi$ should be equals to concentrator FOV.

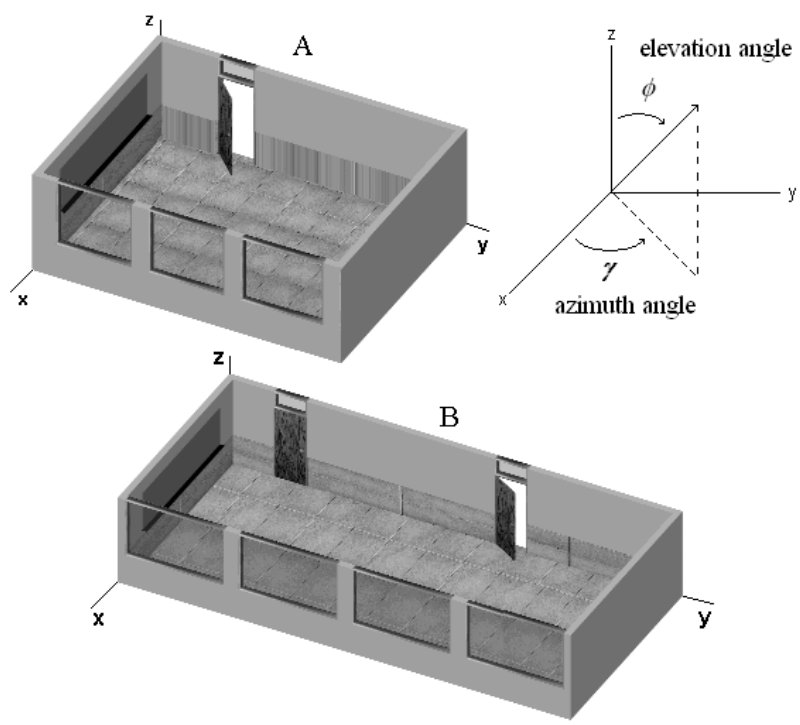

Fig. 2. Graphical representation of A and B classroom.

4. RESULTS

The algorithm described in the previous section including the angle diversity conventional receiver' model was implemented. Following, several simulations results obtained for different optical links are reported, which are characterized by the use of conventional receivers using angle diversity. Using these results, it is possible to establish those parameters of the receiver structure that better performances present with respect to the IR channel features.

Table 1. Simulation parameters

Parameter		A	B
Classroom:	width (x), m	6	6
	length (x), m	7.8	13.14
	height (z), m	2.75	2.75
Emitter:	mode (n)	1	1
	power, W	1	1
	position (x,y,z)	(3,3.9,1)	(3,6.57,1)
Receiver:	active area, cm^2	1	1
	position (x,y,z)	(-,-,1)	(-,-,1)
Concentrator:	*FOV*	ψ_c	ψ_c
	refractive index	1.8	1.8
	exit aperture, cm	0.56	0.56
Bandpass filter:	number of layers	20	20
	peak transmission (T_0)	0.92	0.92
	effective index (n_s)	2.293	2.293
	filter order (m)	3	3
	angular bandwidth ($\Delta\psi$)	ψ_c	ψ_c
Resolution:	Δt, ns	0.2	0.2
Bounces:	k	20	20
Materials	ρ	r_d	m
Wood	0.63	0.6	3
Varnished W.	0.75	0.3	97
Cement	0.40	1	---
Ceramic floor	0.16	0.7	20
Glass	0.03	0	280

4.1 Effect of receiver parameters

In order to investigate the effects of the parameters of a conventional receiver composed by several IR detectors with filter and CPC, such as its FOV and the reception direction, on the path loss and the *rms* delay spread, the IR signal propagation in the classroom B has been examined. Fig. 2 shows the graphical representation of classroom and Table 1 the parameters used for the simulations. The emitter is located at the centre of the classroom aimed towards the ceiling and the detector is located at three meters from the emitter, in the southwest direction on the diagonal: $x=5.2$ e $y=4.4$.

To investigate the rotation effects on the received signal, the azimuth angle, γ, was changed from 0º to 360º in steps of 36º for an specific elevation angle of ϕ=30º (see Fig. 2). Figs. 3(a) y (b) display the *rms* delay spread and the path loss, respectively, for each of the selected azimuth angles for several FOVs: 20º, 30º, 40º, 50º, 70º y 90º. For FOVs from 20º to 70º, a CPC with 1.8 refractive index and 5.64 mm exit aperture were considered, while a FOV=90º indicates that an hemispheric lens was used.

Independently of the field of view, the losses are minimal for a 135º azimuth angle, since for this angle the receiver is facing the centre of the ceiling, where nearly all of the radiation is coming from. Also note how, for this orientation, the use of receivers with a reduced FOV provides a more power-efficient link, due mainly to the increased gain offered by the concentrators with a reduced FOV. The greatest losses, however, are obtained with the receiver facing towards the corner of the room and with reduced FOVs, since receivers with a wide FOV are more power efficient since they gather all the radiation coming in from multiple directions. The minimum of the curves that define the delay spread, Fig. 3(a), matches that of the propagation losses, γ=135º, since at this orientation almost all of the power reaching the receiver from the emitter does so after just one reflection. As the receiver is oriented away from the centre of the ceiling in the room,

the number of duplicates of the original signal arriving at the receiver with different propagation times escalates, which leads to an increase in the time spread. This increase is proportional to the FOV of the receiver.

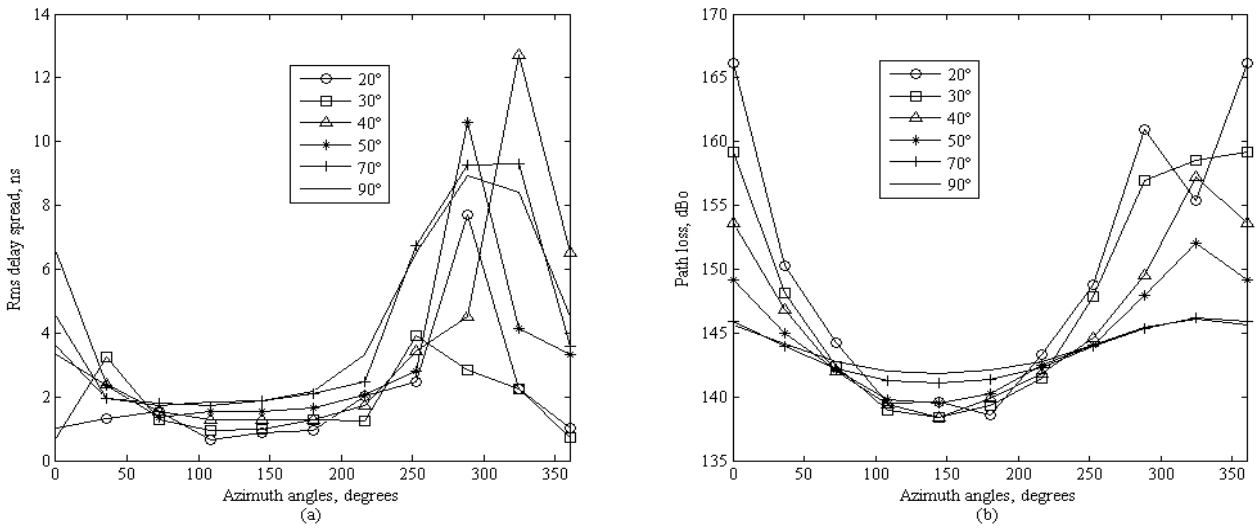

Fig. 3. Channel parameters as a function of azimuth angle for a 30º elevation angle and several FOVs. (a) *Rms* delay spread. (b) Path loss.

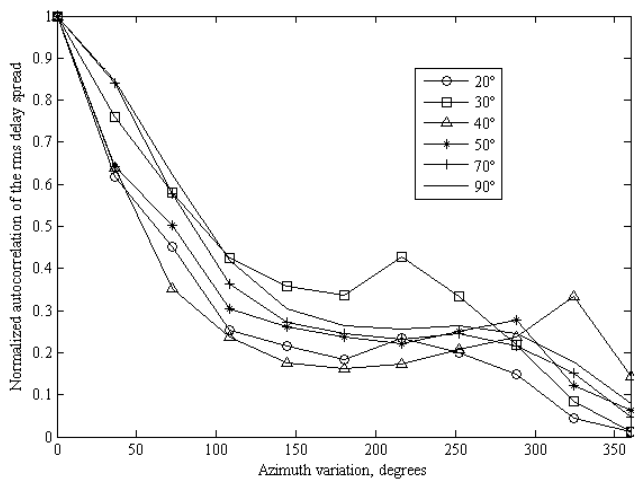

Fig. 4. Normalized autocorrelation of the *rms* delay spread for a 30º elevation angle and several FOVs.

Furthermore, the normalized autocorrelation of the *rms* delay spread has been calculated, which allows us to describe the relation between the features seen by the receiver and its FOV. The curves corresponding to the normalized autocorrelation show how correlated are the channel *rms* delay spread when rotating the receiver by *n* degrees in azimuth (see Fig. 4). For an elevation angle of 30º, and assuming that a new channel[13] is seen by the receiver when the correlation drops below 0.4, and choosing a FOV=50º, we can have independent branches or detectors of a conventional receiver using angle diversity at angular separations of 66.2º. That is, under said conditions, as the receiver's azimuth angle is rotated, it can distinguish among 360/66.2º≅5 channels with different characteristics. From this result, the number of detectors or branches for a conventional receiver using angle diversity could be established if each of them were oriented at a 30º elevation angle and equipped with a 40º FOV concentrator. Table 2 shows the number of elements that would be obtained for each of the FOVs studied. In principle, it is expected that as the FOV is increased, the number of elements decreases. Though this is usually the case, such an inverse proportionality is not guaranteed. For example, for a 40º FOV, the number of independent channels is greater than for 30º. From the resulting data, it can be observed that if an hemispheric lens (FOV=90º) with three branches separated by 114.4º is used for the IR detector, three azimuth independent channels are available.

With the same configuration as that used for the azimuth study, the elevation angle was varied from 0º to 90º in steps of 10º, and the channel parameters for the same FOVs were calculated. As with the azimuth study, the curves that define the normalized autocorrelation of the *rms* delay spread for each FOV allow for a determination to be made of the degree of similarity of the channels seen by each detecting element and its FOV as the elevation angle is varied. Table 3 shows the number of detectors that give rise to channels with different characteristics as a function of FOV and for a 180º azimuth angle. Likewise, it follows that the number of elements in elevation is similar when using either an hemispheric lens or a CPC with a FOV greater than 20º. This result is only valid for the azimuth angle in question, however. In brief, for a 30º elevation angle and a 40º FOV, if elements are oriented every 62.2º in azimuth, five channels with different characteristics will be available, while for a 180º azimuth angle and the same FOV, if the elements are separated 42.2º in elevation, two independent channels will result.

Table 2. No. of elements obtained as a function of FOV for a 30º elevation angle.

FOV	Azimuth variation	No. of elements
20º	81.5º	4
30º	121.1º	3
40º	66.2º	5
50º	90.4º	4
70º	101.9º	3
90º	114.4º	3

Table 3. No. of elements obtained as a function of FOV for a 180º azimuth angle.

FOV	Elevación variation	No. of elements
20º	15.5º	6
30º	37.9º	2
40º	42.2º	2
50º	42,0º	2
70º	40.4º	2
90º	44.0º	2

4.2 Study for the design of a conventional receiver using angle diversity.

A study of the dependence of the IR cannel characteristics on the parameters that define the structure of a conventional receiver using angle diversity provided a procedure for selecting the location of the detectors or branches of the receiver so as to yield channels with different characteristics (independent channels). The results of the study detailed in the previous section, however, are only valid for the receiver location considered, namely the southwest corner of classroom B. Moreover, the angular arrangement of the elements was obtained following an azimuth study carried out for a specific elevation angle of 30º, and an elevation study for a specific azimuth angle of 180º. If a structure completely independent of receiver location and valid for all elevation and azimuth angles is desired, the analysis must be extended to consider all possible receiver positions and elevation and azimuth angles. So as to gather the necessary data to conduct such a study, multiple simulations were carried out using the environment provided by the two classrooms shown in Fig. 2. The emitter was placed in the centre of each room, oriented vertically towards the ceiling, and the receiver was moved, forming concentric circles around the emitter's position. Eight uniformly distributed positions were analyzed on each circle, spaced 0.5 m apart, and the impulse response was determined for receivers with FOVs from 10º to 90º in steps of 10º for 100 different orientations. The remaining parameters used in the simulations matched those shown in Table 1. As in the previous section, and based on the measurement plan presented, we conducted a study of the dependence of the channel characteristics on the FOV and orientation of a detecting element.

Figs. 5(a) and (b) show, respectively, the average and standard deviation of the angular separation in elevation that result in channels with independent characteristics as a function of azimuth angle and for several FOVs. The procedure used to compile the graphs is similar to that used in the previous section. Starting from the normalized autocorrelation for the *rms* delay spread in elevation, we determined the angular separation in elevation required for the *rms* delay spread to fall below 0.4, along with the average and standard deviation of the values obtained for each of the azimuth angles analyzed. Independently of the azimuth angle, the angular separation in elevation that provides independent channels for each FOV is determined by the sum of the maximum of the average angular separation for said FOV and its standard deviation. For

example, for a 20º FOV, the resulting angular separation is approximately 56º in elevation (≅47º+9º). The next step involves selecting the FOV of the detecting elements. Doing so requires determining those parameters that characterize the channel as a function of FOV and elevation angle. Figs. 6(a) and (b) show, respectively, the average *rms* delay spread and path loss as a function of elevation angle and several FOVs. These curves were prepared after analyzing all the orientations in azimuth for each possible receiver position within the two classrooms. The curves allow us to deduce that elements with small FOVs result in lower *rms* delay spread and path loss values than those with high FOVs. As an example, note that using an hemispheric lens, FOV=90º, is the best option for those elements with orientations close to 90º, and the worst when dealing with elevations near 0º (from the vertical). For large elevation angles, an hemispheric lens yields a lower rms delay spread and path loss than a CPC. In general, in order to obtain a conventional receiver using angle diversity with similar elements, CPCs with a 50º FOV should be used, as this offers the best compromise in both parameters regardless of the elevation angle in question.

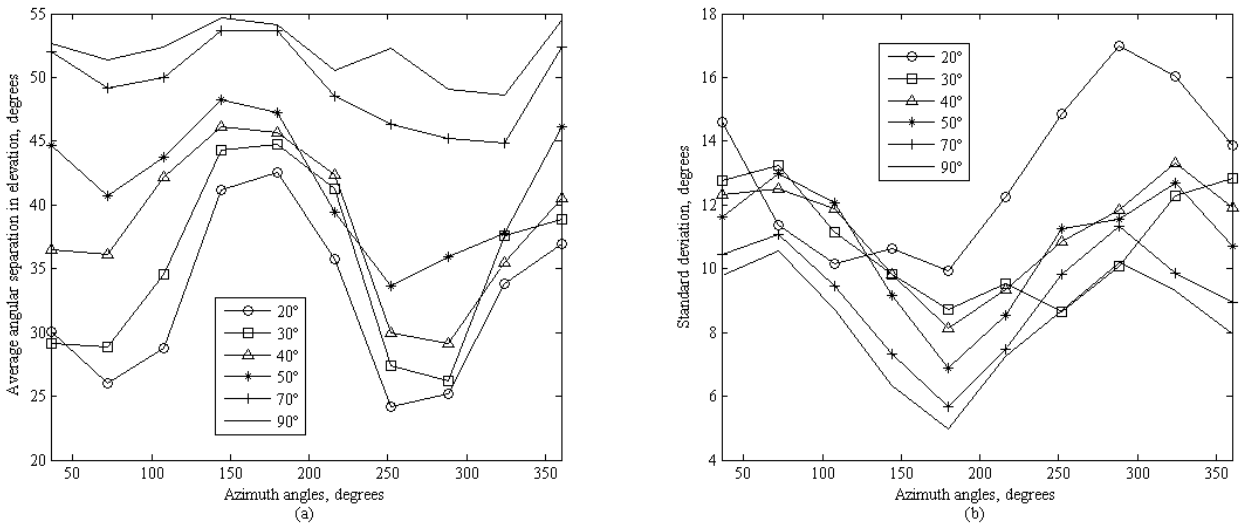

Fig. 5. Elevation study as a function of azimuth angle for several FOVs. (a) Average angular separation in elevation that yields independent channels. (b) Standard deviation.

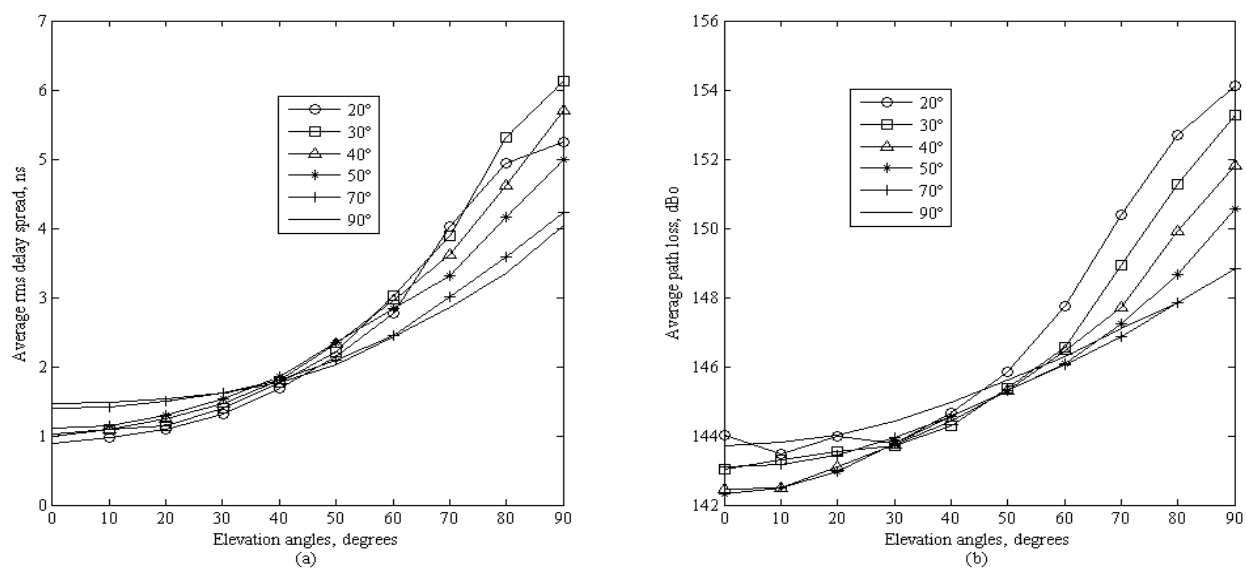

Fig. 6. Channel parameters as a function of elevation angle for several FOVs. (a) Average *rms* delay spread. (b) Average path loss.

A similar procedure for the study in elevation was exectuted in azimuth. According to the obtained results and assuming that a conventional receiver should have a branch or detector oriented towards the ceiling, because it is the main reflector of power and that must have axial symmetry[3,14], a receiver using angle diversity that relies on the use of concentrators with a 50º FOV must consist of seven detectors, one oriented vertically towards the ceiling, with the other six, uniformly distributed in azimuth, forming a 56º angle with respect to the vertical element.

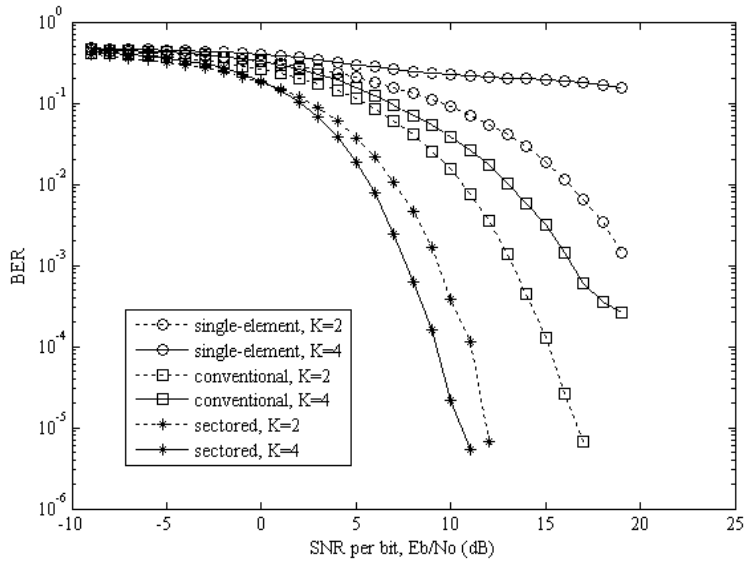

Fig. 7. BER for L-PPM ($L=2^K$) modulation schemes at 50 Mbps against the SNR per bit.

In order to study the proposed structure in a representative link budget, the performance of Pulse-Position Modulation (PPM) has been evaluated and compared with other receiver using angle diversity, the sectored receiver propose by Mendoza[15], and a receiver using a single-element detector with a FOV=90º. The sectored receiver is compoused by three crowns of four, four and eight sectors or detectors, respectively. For the three receivers, the channel responses were calculated with the receiver located 3 meters from the emitter, inside the classroom A (see Fig. 2). Table 1 shows the parameters used for the simulations. To obtain the output of the angle diversity receivers (the combined channel response), a selection combining method was implemented, where the element with the lowest delay spread is selected[6]. PPM is an orthogonal modulation scheme that offers a decrease in average power requirement to achieve a desired bit error rate (BER) compared to On-Off Keying, at the expense of an increase bandwidth requirement[1]. L-PPM utilizes symbols consisting of $L=2^K$ time slots, which we will refer to as chips. A constant power LP_E is transmitted during one of these chips and zero power is transmitted during the remaining L-1 chips, thereby encoding $K=\log_2 L$ bits in the position of the "high" chip. For a given bit rate, L-PPM yields an average power requirement that decreases steadily with increasing L. In the absence of multipath distortion, an optimum maximum-likelihood receiver for L-PPM employs a continuous-time filter matched to one chip, whose output is sampled at the chip rate. Each block of L samples is passed to the block decoder, which makes a symbol decision, yielding K information bits. In soft decision decoding, the samples are unquantized, and the block decoder chooses the largest of the L samples. When L-PPM is transmitted over multipath channels, such as wireless optical channels, the nonzero transmitted chips can induce interference in chips both within the same symbol (intrasymbol interference) and in adjacent transmitted symbols (intersymbol interference): we will refer these effects collective as ISI. Fig. 7 displays the BER as a function of the signal to noise ratio (SNR) per bit, E_b/N_0, for the three receivers employing 4-PPM (K=2) and 16-PPM (K=4) systems at 50 Mbps. The receivers are used for systems employing no equalization, i.e., using the same receiver filter and soft decision decoder that is optimal on a distortionless channel. Comparing the results, we can observe that sectored receiver and the single-element detector yield the best and the worst performance, respectively. Although the sectored receiver presents better BER than the conventional receiver, its implementation is more complex. The sectored receiver is composed of sixteen detectors or photodiodes, while the conventional is composed of just seven.

5. CONCLUSIONS

A simulation tool for the fast calculation of the impulse response of the IR indoor channel has been developed, that allows us to simulate the behaviour of different link configurations. It incorporates the Phong's model to approximate the reflection pattern of those indoor surfaces that present a specular component. The use of angle-diversity receivers may be used to benefit the design of high performance IR systems. For this reason, we have presented a model for the effective signal-collection area of a conventional receiver using angle diversity upon which a Monte Carlo based ray-tracing algorithm allows us to analyze and to study those optical links that are characterized by the use of these receivers and investigate the structure of the conventional receiver that yields improve performance with respect to the IR channel parameters: the path loss and the *rms* delay spread. Assuming that a conventional receiver using angle-diversity has a branch oriented towards the ceiling, we can recommend a conventional receiver with seven receiving element or photodiodes. One oriented towards the ceiling, and six looking at an elevation of 56º with a separation of 60º in azimuth. For each element, a CPC with a FOV=50º must be used. Furthermore, the proposed structure was evaluated in a representative link budget using L-PPM modulation schemes and its performance is compared with other angle-diversity receiver and a receiver using a single-element detector with a FOV=90º.

ACKNOWLEDGEMENTS

This work has been funded in part by the Spanish Research Administration (TEC2006-13887-C05-05).

REFERENCES

[1] Kahn, J.M., and Barry, J.R., "Wireless Infrared Communications", Proceedings of the IEEE 85(2), 367-379 (1997).

[2] Al-Ghamdi, A.G.., Elmirghani, J.M.H., "Analysis of Diffuse Optical Wireless Channels Employing Spot-Diffusing Techniques, Diversity Receiveres, and Combining Schemes", IEEE Transactions on Communications 52(10), 1622-1631 (2004).

[3] Carruthers, J.B., and Kahn, J.M., "Angle Diversity for Nondirected Wireless Infrared Communication", IEEE Transactions on Communications 48(6), 906-969 (2000).

[4] Jivkova, S., Hristov, B.A., Kaverhrad, M., "Power-Efficient Multispot-Diffuse Multiple-Input-Multiple-Output Approach to Broad-Band Optical Wireless Communications", IEEE Transactions on Vehicular Technology 53(3), 882-888 (2004).

[5] Djahani, P., and Kahn, J.M., "Analysis of Infrared Wireless Links Employing Multibeam Transmitters and Imaging Diversity Receivers", IEEE Transactions on Communications 48(12), 2077-2088 (2000).

[6] Lomba, C.R.A.T., Valadas, R.T., Oliveira Duarte, A.M., "Sectored Receivers to Combat the Multipath Dispersion of the Indoor Optical Channel", PIMRC'95 6, 321-325 (1995).

[7] Barry, J.R., Kahn, J.M., Lee, E.A., Messerschmitt, D.G., "Simulation of Multipath Impulse Response for Indoor Wireless Optical Channels", IEEE Journal on Selected Areas in Communications 11(3), 367-379 (1993).

[8] López-Hernández, F.J., and Betancor, M.J., "DUSTIN: a Novel Algorithm for the Calculation of the Impulse Response on IR Wireless Indoor Channels", Electronic Letters 33(21), 1804-1805 (1997).

[9] López-Hernández, F.J., Pérez-Jiménez, R., and Santamaría, A., "Ray-Tracing Algorithms for Fast Calculation of the Channel Impulse Response on Diffuse IR-Wireless Indoor Channels", SPIE Optical Eng. 39(10), 1510-1512 (2000).

[10] Rodríguez, S., Pérez-Jiménez, R., López-Hernández, F.J., González O., Ayala, A., "Reflection model for calculation of the impulse response on IR-wireless indoor channels using ray-tracing algorithm", Microwave and Optical Technology Letters 32(4), 296-300 (2002).

[11] Rodríguez S., Pérez-Jiménez R., López-Hernández F.J., González O., Mendoza B.R., "Models and Algorithm for the calculation of the impulse response on IR wireless indoor channels", Proc. SPIE 5117, 199-208 (2003).

[12] Barry, J.R., Kahn, J.M., "Link Design for Nondirected Wireless Infrared Communications", Applied Optics 34(19), 3764-3776 (1995).

[13] Pakravan, M.R., Kaverhad, M., "Design Considerations for Broadband Indoor Infrared Wireless Communication Systems", International Journal of Wireless Information Networks 2(4), 223-237 (1995).

[14] Jivkova, S.T., Kavehrad, M., "Multispot diffusing configuration for wireless infrared access", IEEE Transactions on Communications 48(6), 970-978 (2000).

[15] Mendoza, B.R., Rodríguez, S., Pérez-Jiménez, R., González, O., Poves, E., "Considerations on the design of sectored receivers for wireless optical channels using a Monte Carlo based ray tracing algorithm", IET Optoelectronics 1(5), 226-232 (2007).